VERIFICATION AND VALIDATION STUDY OF OPENFOAM ON THE GENERIC PRISMATIC PLANING HULL FORM

JIAHUI LI*, LUCA BONFIGLIO† AND STEFANO BRIZZOLARA*

*iShip lab., Department of Aerospace and Ocean Engineering
Virginia Tech
420 Old Turner Street, Blacksburg, VA 24061, USA.
e-mail: jiahui37@vt.edu; stebriz@vt.edu

† MIT-Sea Grant College Program
Massachusetts Institute of Technology
12 Emily St. NW98-180, Cambridge, MA 02139, USA
e-mail: bonfi@mit.edu

Key words: Planing hulls, GPPH, OpenFOAM, URANS

Abstract. The paper presents the first series of results obtained in an ongoing validation and verification study of inter-dynamic OpenFOAM solver framework on a new set of high quality experimental tests performed on a large (2.4m long) generic planing hull model (GPPH) with high deadrise (18deg), from the pre-planing (Fn_∇=2.6) to fully planing (Fn_∇=5.7) regimes. This test case is a good benchmark for the free surface capturing model implemented in OpenFOAM which is based on a rather simple transport equation for an additional scalar field that defines the fraction of water in each cell of the computational mesh. This model, in spite of its simplicity seems capable of reproducing complex violent free surface flows such as that observed in planing hulls, that includes jet spray forming on the bottom and detaching from the chine of the planing hull and overturning waves off the wet chine region, with some nuances. The dependence of the flow solution on the mesh quality is presented and discussed. Practical indication of the level of uncertainty of CFD models for the prediction of the calm water hydrodynamics of the GPPH is given at the highest simulated speed. Predictions are then extended to the whole speed range, including dynamic trim and sinkage.

1 INTRODUCTION

CFD is taking the place of experimental tests in many engineering fields. In naval architecture, the accuracy and reliability of numerical simulations have been extensively validated with model scale experiments performed on different displacement hull forms [1] and the conclusion is that RANSE solvers are a mature tool for displacement ship design.

Validation and Verification (V&V) studies for high speed planing crafts are very less in comparison with larger displacement hull forms and often lack of high quality experimental

reference data on modern hull forms. Previous validation studies have considered old systematic planing hulls series [2] [3] that hardly reflect contemporary planing hull forms. Only few studies have considered modern planing hull shapes for practical seagoing application [4] [5] [6].

In the case of planing crafts, the free surface flow regime changes completely with respect to displacement hulls. The free waves patterns loose importance while the accurate estimation of the dynamic pressure distribution on the hull due to a water entry like flow becomes essential. In fact, the dynamic equilibrium of the vessel derives from the accurate prediction dynamic forces (mostly dynamic lift and not buoyancy) acting on the dynamic wetted portion of the planing hull. Hence, it can be argued that the running attitude of planning craft might be strongly dependent on the mesh resolution close to hull regions interested by jet spray formations such as the fore body (spray root line), chine and transom where flow separation phenomena occur.

In fact recent studies have appeared correct modeling of the non-linear free surface dynamics [4] even in presence of steps and ventilation [5]. The significant pressure field on the hull surface due to high Froude number and the sharp edges characterizing both the chine and the transom of planing craft induce jet sprays that need to be correctly modeled to achieve high accuracy in the prediction of the hydrodynamic forces exerted on the hull.

Under this perspective, the study aims to investigate the performance of the standard OpenFOAM solver interdymfoam, which combines mesh morphing to allow for the hull kinematic and a volume of fluid solver based on a rather simple transport equation for an additional scalar field that defines the fraction of water in each cell of the computational mesh. This model, in spite of its simplicity seems capable of reproducing complex violent free surface flows (see for instance [7]), such as that observed in planing hulls, that includes jet spray forming on the bottom and detaching from the chine of the planing hull and overturning waves off the wet chine region. The Validation and Verification study on the GPPH hull at the highest speed presented in this paper, shows that for planing hulls the flow mixture predicted by the volume of fluid solver is highly dependent on the mesh quality and refinement in high pressure regions. Typical problems noted by other researchers [2] [3] such as numerical (non-physical) diffusion of air under the hull, are noted also in this case and systematically addressed by the V&V study at the highest speed. The CFD predictions of resistance, dynamic trim and sinkage are then extended to the whole pure planing speed range (Fn_∇ = 4.2 - 5.7) in the last section.

2 PHYSICAL AND NUMERICAL MODEL

The numerical model proposed in the present study is based on the solution of the Unsteady Reynolds Averaged Navier Stokes equations. The system is a set of partial differential non linear equations in the unknows of pressure and velocity components. The physical problem is described in terms of mass and momentum conservation equations which are solved in a Cartesian reference frame for the pressure and velocity unknowns:

$$\begin{aligned} &\frac{\partial(\rho u_i)}{\partial x_i} = 0, \\ &\frac{\partial u_i}{\partial t} + \frac{\partial(u_i u_j)}{\partial x_j} = \frac{\partial}{\partial x_j}(\nu \frac{\partial u_i}{\partial x_j}) - \frac{1}{\rho}\frac{\partial p}{\partial x_i} + g_i. \end{aligned} \tag{1}$$

Even in model scale, the fluid dynamic problems considered in the present study is characterized by a high Reynolds number ($R_E \in [1e7, 3e7]$) inducing fully turbulent flow. We solve the fluid

dynamic problem by applying a Reynolds averaging technique to the solution of N-S equations. In particular, we have used the $k-\omega$ turbulence model (see [8]) reformulated in the Shear Stress Transport version (SST) by [9, 10]) with the goal to improve the model independence from freestream turbulent intensity through a formulation which blends the k-ϵ model (used in the free stream) and the k-ω model (used in the boundary layer). Freestream values of the turbulent quantities are calculated according to the turbulent intensity and length scale based on the flat plate boundary layer thickness formulation:

$$k = \frac{3}{2}(UI)^2 \qquad \omega = \frac{k}{\nu_T} \qquad \nu_T = \frac{1}{\rho}\sqrt{\frac{3}{2}}UIl \tag{2}$$

In equation (2) l indicates the turbulent length scale and has been selected according to the boundary layer thickness δ_{99} of a turbulent flow on a flat plate.

$$l = 0.4\delta_{99} \qquad \frac{\delta_{99}}{L} = \frac{0.374}{Re^{\frac{1}{5}}} \tag{3}$$

A volume of Fluid (VOF) surface capturing technique ([11]) is here used to predict the wave pattern generated by the hull advancing at the free surface. URANS equations are solved for a fluid mixture of water and air whose characteristics are determined on the basis of the scalar function γ:

$$\rho = (1-\gamma)\rho_W + \gamma\rho_A \tag{4}$$

$$\mu = (1-\gamma)\mu_W + \gamma\mu_A \tag{5}$$

At each time-step the local value of γ is determined by the solution of the following equation:

$$\frac{\partial\gamma}{\partial t} + \nabla\cdot(\gamma U) + \nabla\cdot[\gamma(1-\gamma)U_r] = 0 \tag{6}$$

In equation (6) the term U_r indicates the relative velocity between water and air and it is here used to steepen the gradient of the VoF scalar function γ close to the interface. U_r is tuned through the parameter C_f as follow:

$$Ur = n_f \min\left[C_f\frac{\phi}{S_f}, \max\left(\frac{\phi}{S_f}\right)\right] \tag{7}$$

In particular $\nabla\cdot[\gamma(1-\gamma)U_r]$, also called artificial compression, is effective when $\gamma \neq 0$ and $\gamma \neq 1$ and it is opportunely tuned to increase the compression of the free surface hence reducing the interface smearing often experienced when surface capturing techniques are used to predict free surface flows.

A constant flow velocity is imposed at the inlet according to the specific operating conditions. Neumann boundary condition is used for the dynamic pressure field at the inlet (zero gradient). Constant zero dynamic pressure is enforced at the outlet of the computational domain where a Neumann boundary condition is instead used for the velocity field (zero gradient). No-slip condition is imposed at the hull surface where a zero gradient dynamic pressure condition is used together with a zero velocity field. Top, bottom and side boundaries have been modeled as slip walls.

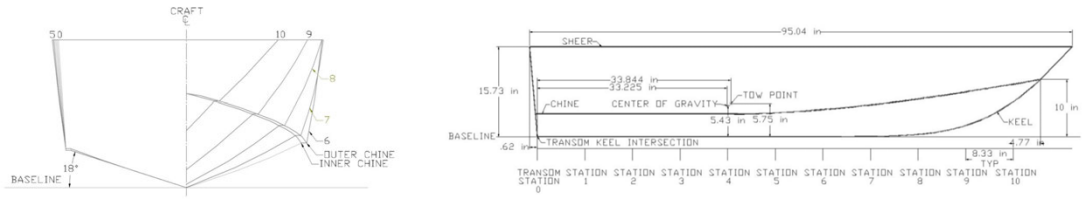

(a) GPPH Body Plan (b) GPPH Profile

Figure 1: GPPH Test Model [14]

Ship motion is obtained using a dynamic mesh strategy supported by grid morphing algorithm that diffuse boundary motion through internal grid points. Mesh motion is computed from the pressure field on the hull. In particular, at each time-step the position and the velocity of the hull are known as well as the forces and moments acting on the rigid body (which result from pressure and velocity fields integration). We solve the forward dynamic problem using a 6 Degrees of Freedom solver in which surge, sway, roll and yam motions are constrained, while heave and pitch accelerations are computed using a Newmark solver (see [12]). A pseudo-solid Laplace smoothing equation distributes hull motion to the internal grid points through a diffusivity coefficient Γ following equations (8) and (9):

$$\nabla \cdot (\Gamma \nabla V) = 0 \tag{8}$$

Once mesh deformation velocity (V) is known at each point, grid displacement is found at each new time step t^n solving a linear motion equation:

$$x_n = x_{n-1} + V\Delta t \tag{9}$$

Equation (9) describes the deformation of an initially valid mesh (t_{n-1}) into a deformed mesh at t_n. The quality of the grid is verified at each time step to ensure that no faces and no cells were inverted during motion. This method has been applied with success for the solution of forced oscillation problems (see [13])

The numerical solution of the aforementioned physical problem is obtained using a Finite Volume approach with collocated arrangement of variable. In particular, we have used OpenFOAM libraries to numerically solve the non-linear system of PDEs describing the fluid dynamic problem on a computational domain discretized through unstructured grid (see [15]). More in details, the solution of the dynamic pressure term is here obtained using an algebraic multigrid method (*GAMG* - Geometric Algebraic Multi Grid) with a *DIC* (Diagonal Incomplete Cholesky) smoother. The tolerance has been set up to 5e-8. Velocity U and transported quantities (turbulent kinetic energy k and specific dissipation rate ω terms) have been solved using a smooth solver suitable for asymmetric matrices with a symmetric Gauss Seidel smoother with a tolerance of 1e-7. Volume of fluid term γ, has been solved with a smooth solver used also for other transported quantities, but in this case we have used a MULti-dimensional Limiter for Explicit Solution (MULES) to guarantee boundedness of γ. The tolerance has been constrained to 1e-10 and the artificial compression of the free surface (see (7)) has been tuned through the parameter C_f (C_f=1). This solver is particularly effective when used in combination with an adjustable

Table 1: Tested GPPH Characteristics

Parameter	Value
Length Between Particulars, L_{pp}	2.4140 (m)
Maximum Projected Chine Beam, B_{PX}	0.6274 (m)
Deadrise Angle to Outer Chine, β	17.2000 (degree)
Displacemet, ∇	101.5140 (kg)
Longitudinal Center of Gravity, LCG	0.8439 (m)
Vertical Center of Gravity, VCG	0.1379 (m)
Longitudinal Center of Tow Point, LTP	0.8596 (m)
Vertical Center of Tow Point, VTP	0.1461 (m)
Hydrostatic Draft at Transom Above Baseline, $T_{Transom}$	0.1476 (m)
Hydrostatic Trim Angle from Baseline (+bow↑)	0.1270 (degree)

time-step strategy that at each time iteration select the time-step in order to satisfy a given constraints on the Courant number, which in a 1-D case is defined as:

$$Co = u\frac{\Delta t}{\Delta x} \tag{10}$$

In particular, the unsteady solution of RANS equations is achieved differentiating in time with an implicit Euler scheme and adjustable time step selected according to the maximum Courant number ($Co < 0.5$ at the free surface and $Co < 1$ everywhere else). Navier-Stokes equations have been solved including gravity effects but dropping the hydrostatic component from the pressure field. The pressure-velocity coupling is here solved using the PISO scheme.

3 TEST CASE

The test model of Generic Prismatic Planing Hull is designed by the Naval Surface Warfare Center as assessment for CFD simulation tools. This model uses a modern planing hull bow shape and a prismatic hull aft of the bow area to minimize the geometric variables, thus to have the physics and response to waves of a typical planing hull. [14] The test data used in this paper is from the November 2015 test performed at Naval Surface Warfare Center Carderock Division (NSWCCD). Figure 1(a) shows the body plan of the model, Figure 1(b) shows profile view of the model.

The model is only allowed to be free to heave and pitch while it was restrained in surge, sway, roll and yaw by the experimental setup. The model was tested under 7 different speeds from pre-planing to fully planing regimes.

4 VERIFICATION & VALIDATION STUDY

The solution of the physical problem described in section 2 is obtained through a finite volume numerical technique with collocated arrangement of variables. Figure 3 presents RANSE predictions obtained at V=12.24 m/s corresponding to the highest volumetric Froude number tested by [14] ($F_\nabla = \frac{V}{\sqrt{g\nabla^{1/3}}}$=5.723). The accuracy of the numerical solution depend on the

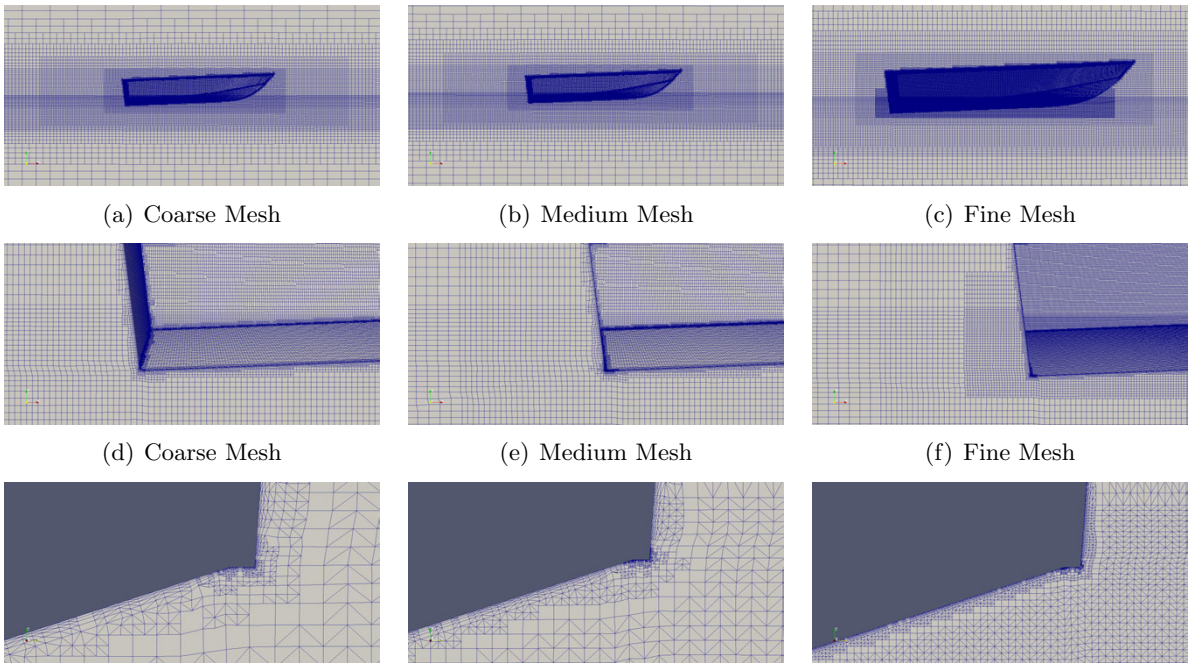

(a) Coarse Mesh (b) Medium Mesh (c) Fine Mesh

(d) Coarse Mesh (e) Medium Mesh (f) Fine Mesh

(g) Coarse Mesh (h) Medium Mesh (i) Fine Mesh

Figure 2: Overview of the three numerical grids used for the grid verification and numerical uncertainty estimation study. Top three panels (2(a),2(b) and 2(c)) present a longitudinal view of the grid including the hull and the surrounding free surface region). Middle panels (2(d),2(e) and 2(f)) show grid refinements in proximity of the flat transom. Bottom panels (2(g),2(h) and 2(i)) present grid refinements on the hull bottom with specific focus to the chine region.

Table 2: Numerical Results obtained with the three meshes at the highest speed V=12.24 m/s

	Coarsest Mesh	Relative Error (%)	Medium Mesh	Relative Error (%)	Fine Mesh	Relative Error (%)	Experimental Result	Savitsky Short Method
Mesh (Number of Cells)	1141900	—	2424676	—	4560229	—	—	—
Grid step size (h_i)	1.587	—	1.234	—	1	—	—	—
Resistance [N]	220.4	18.32	244.0	9.57	252.0	6.61	269.83	231.32
Friction Drag [N]	158.0	—	182.1	—	190.0	—	—	181.98
Pressure [N]	62.4	—	61.9	—	62.0	—	—	49.34
Trim Angle [degree]	1.87	34.15	2.14	1.46	2.19	1.08	2.17	2.84
Heave [cm]	10.32	7.54	9.99	4.08	9.89	3.14	9.60	10.33
L_C [cm]	43.45	2.25	43.11	3.01	42.97	3.55	44.45	50.54
L_K [cm]	168.94	2.19	173.21	0.28	174.01	0.74	172.72	175.31

numerical set-up and the strategy adopted for the discretization of the computational domain. In this section we describe the grid generation strategy and we present a verification study having the goal to characterize the uncertainty of the numerical solution.

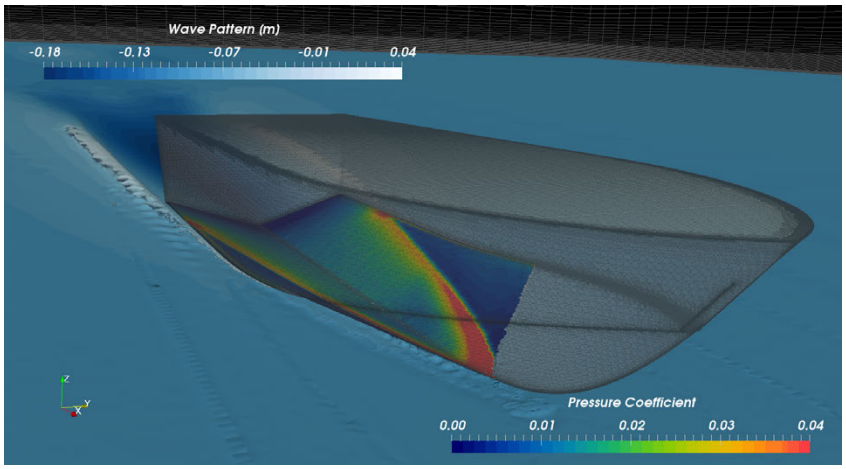

Figure 3: Perspective view of the pressure coefficient contours on the bottom of the planing hull. Red color indicate the spray root line. Blue colors indicate the wave pattern at V=12.24 m/s. Results obtained using the medium mesh described in table 2.

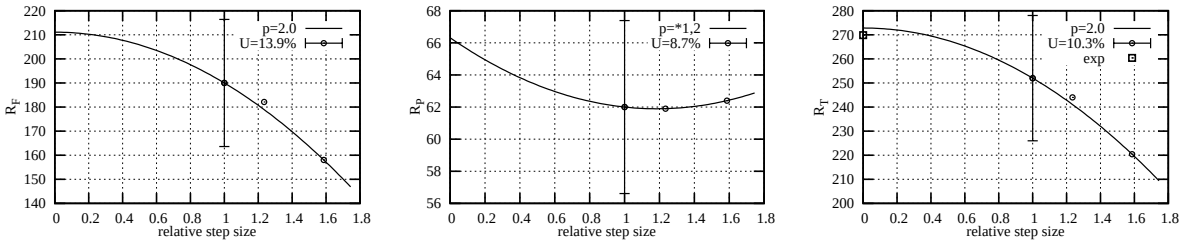

(a) Friction Resistance (b) Pressure Resistance (c) Total Resistance

Figure 4: Convergence of the friction (4(a)), pressure (4(b)) and total (4(c)) calm water resistance with respect to the relative step size $\frac{h_i}{h_1}$ defined in equation (11).

4.1 Grid Generation Strategy

The computational domain covers a total length of 36.21 m, corresponding to 15 ship lengths, a total breadth of 36.21 and a total height of 9.242 m. With reference to a Cartesian coordinates system (xyz), the tow point of the planing hull is positioned at (0,0,0). The longitudinal distance between the tow point and inlet is 12.07 m, corresponding to 5 ship lengths. The bottom of the domain is positioned at 7.242 m, corresponding to 3 ship lengths, while the top is located at 2 m from the free surface at rest (approximately 1 ship length). The computational domain is divided in 6 vertical regions, each representing a specific depth-wise layer. With reference to the design water line (free surface at rest), three layers are used to discretize the water region while the remaining three are employed in the air region. Each depth-wise region extends from inlet to outlet without any geometrical progression in the length- (x) or breadth-wise (y) direction. Geometrical progressions are used in the bottom and top layer to coarsen the grid resolution from the internal volume to the top and bottom boundaries of the computational domain. We first construct a background mesh of structured elements discretizing the 6 depth-wise layers

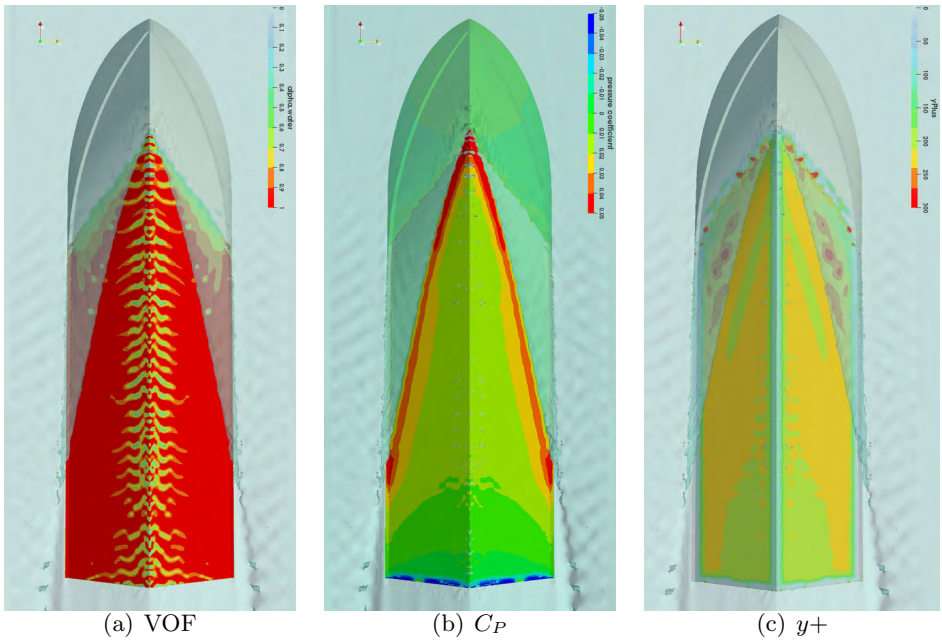

(a) VOF (b) C_P (c) $y+$

Figure 5: Numerical solution obtained using the coarse grid described in table 2. Results presented in terms of Volume of Fluid, pressure coefficient and non-dimensional wall distance contours on the hull bottom. Steady-state solution at V=12.24 m/s.

previously described. This structured grid is successively refined in the $x-y$ direction by iteratively selecting sub-domain regions containing the hull and refining them in the length-breadth direction. The refinement in the direction perpendicular to the free surface is performed only using the aforementioned depth-wise layers for the construction of the structured grid. Refinement in the $x-y$ directions are performed using 6 refinement boxes containing the hull. The plane-wise refinement process leads to an unstructured background grid that is then intersected with the hull surface. The hull is represented by means of a triangulated surface mesh serving as input for the generation the unstructured grid. The hull surface mesh is intersected with the unstructured background grid through an iterative procedure that first increases mesh resolution at the hull-surface/background-grid intersections and then discards cells with centroid inside the hull surface. Cell vertices of this jagged mesh are successively projected on the hull surface and repeatedly extruded in order to obtain layers of prismatic cells suitable for boundary layer flow resolution. The background grid has been constructed using *blockMesh* and successively refined in the $x-y$ direction using six *topoSet-refineMesh* iterative loops. The hull-background intersection has been performed using *snappyHexMesh* utility (see [15] for further details).

4.2 Grid verification

A mesh convergence study is performed at the highest speed, 12.24 m/s corresponding to $Fr_\nabla = 5.75$. The grid verification analysis has the goal to estimate the numerical uncertainty of CFD predictions for friction, pressure and total calm water resistance. To this end, we consider three different computational domain discretizations. With reference to the mesh description

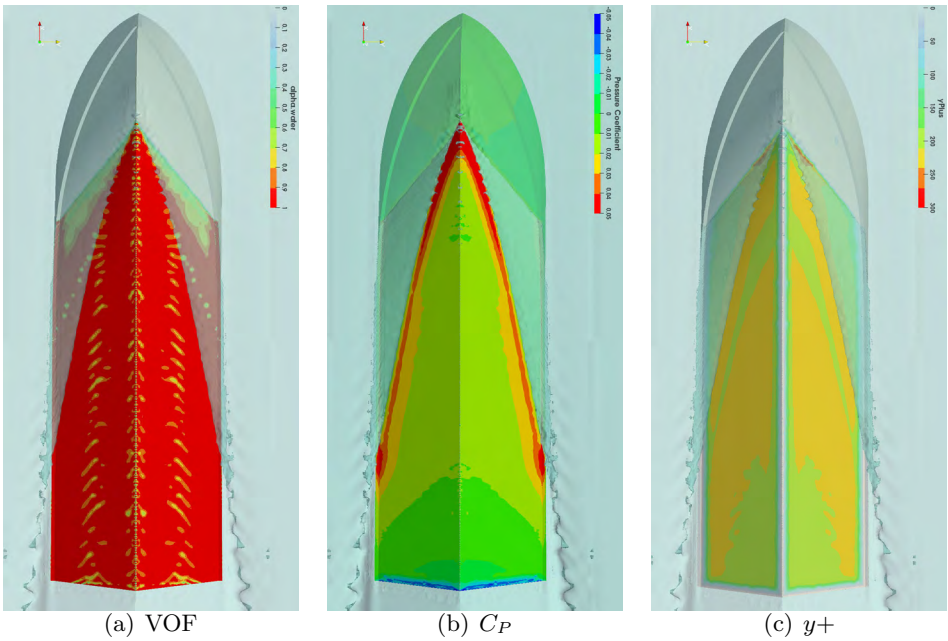

(a) VOF (b) C_P (c) $y+$

Figure 6: Numerical solution obtained using the coarse grid described in table 2. Results presented in terms of Volume of Fluid, pressure coefficient and non-dimensional wall distance contours on the hull bottom. Steady-state solution at V=12.24 m/s.

previously provided, we have systematically increased the resolution of the background grid as well as the mesh resolution in proximity of the hull. During this process we ensured conformity of several mesh quality indicators, such as maximum aspect ratio, number of non-orthogonal faces, maximum skewness. Figure 2 presents a comparison between the three different discretizations used in the grid verification study. Numerical predictions are presented in terms of total resistance as well as shear and pressure drag components in Table 2. At this high Froude number, the prevalent resistance component is the friction drag which accounts for more than 75% of the total resistance. The ration of the two resistance components is confirmed by the estimation obtained with Savitsky short method that are reported in the last column. Apparently the numerical predicted pressure drag does not change considerably with mesh resolution, this is

Uncertainty U and order of convergence p have been estimated using power series expansions as a function of the relative grid size, following the procedure described by [16]. Figure 4 presents convergence of friction resistance (Figure 4(a)), pressure resistance (Figure 4(b)) and total resistance (Figure 4(c)) with respect to grid relative step size defined as follows:

$$\frac{h_i}{h_1} = \left(\frac{n_1}{n_i}\right)^{\frac{1}{3}} \tag{11}$$

Where n_i represents the total number of cells used in the unstructured grids previously presented and n_1 is the total number of cells of the finest grid used in the numerical uncertainty estimation. Grid step size h_i is reported in table 2 for the three grids used in the verification study. Discretization error ϵ is estimated for pressure R_P, friction R_F and total resistance R_T

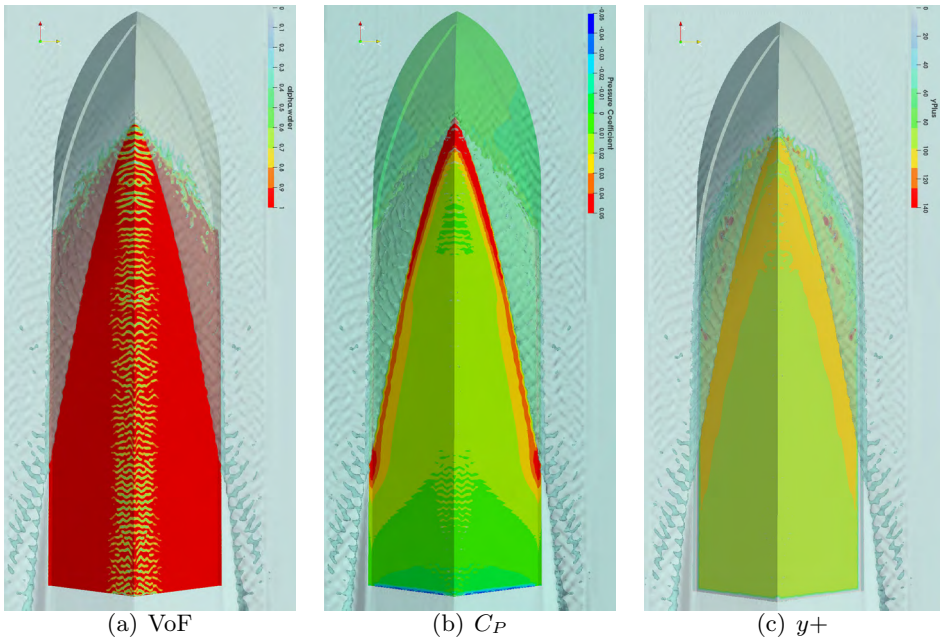

(a) VoF (b) C_P (c) $y+$

Figure 7: Numerical solution obtained using the coarse grid described in table 2. Results presented in terms of Volume of Fluid, pressure coefficient and non-dimensional wall distance contours on the hull bottom. Steady-state solution at V=12.24 m/s.

using the following truncated power series expansion:

$$\begin{aligned} \epsilon_{R_F} &\approx R_{F_i} - R_{F_0} = \alpha h_i^2 \\ \epsilon_{R_P} &\approx R_{P_i} - R_{P_0} = \alpha_1 h_i + \alpha_2 h_i^2 \\ \epsilon_{R_T} &\approx R_{T_i} - R_{T_0} = \alpha h_i^2 \end{aligned} \tag{12}$$

Equation (12) suggest that friction and total resistance are monotonically converging, contrarily from pressure resistance which is instead non-monotonically convergent. The approximate exact solutions for pressure resistance is R_{P_0}= 66.3 N with uncertainty U=8.69%, for friction resistance is R_{F_0}=211.1 N with uncertainty U=13.9% while for total resistance is R_{T_0}=272.8 N with uncertainty U=10.3%. The approximate exact solution for the total resistance present a relative error w.r.t. experiments of about 1%. Despite the polynomial fitting suggest an approximate exact solution for pressure resistance of about 66.3 N with 8.7% of uncertainty, we believe that the discrepancy characterizing CFD predictions of total resistance should be mostly imputed to an inaccurate solution of the friction resistance on the hull bottom. Figure 5, 6 and 7 present CFD results obtained for the coarse, medium and fine mesh as defined in table 2. More in detail, figures 5(a) 6(a) and 7(a) show VOF contours on the hull bottom at the latest time-step (corresponding to a non-dimensional time Ut/L of 16.3). VOF contours as predicted by the coarsest grid (figure 5(a)) present extensive numerical ventilation in proximity of the keel in the pressure area. The medium mesh, characterized by similar values of non-dimensional wall distance $y+ = \frac{u_* y}{\nu}$ (see figures 5(c) and 6(c)), partly mitigate this numerical inaccuracy (see figure 6(a)), however for the finest grid, characterized by lower values of $y+$ (figure 7(c)),

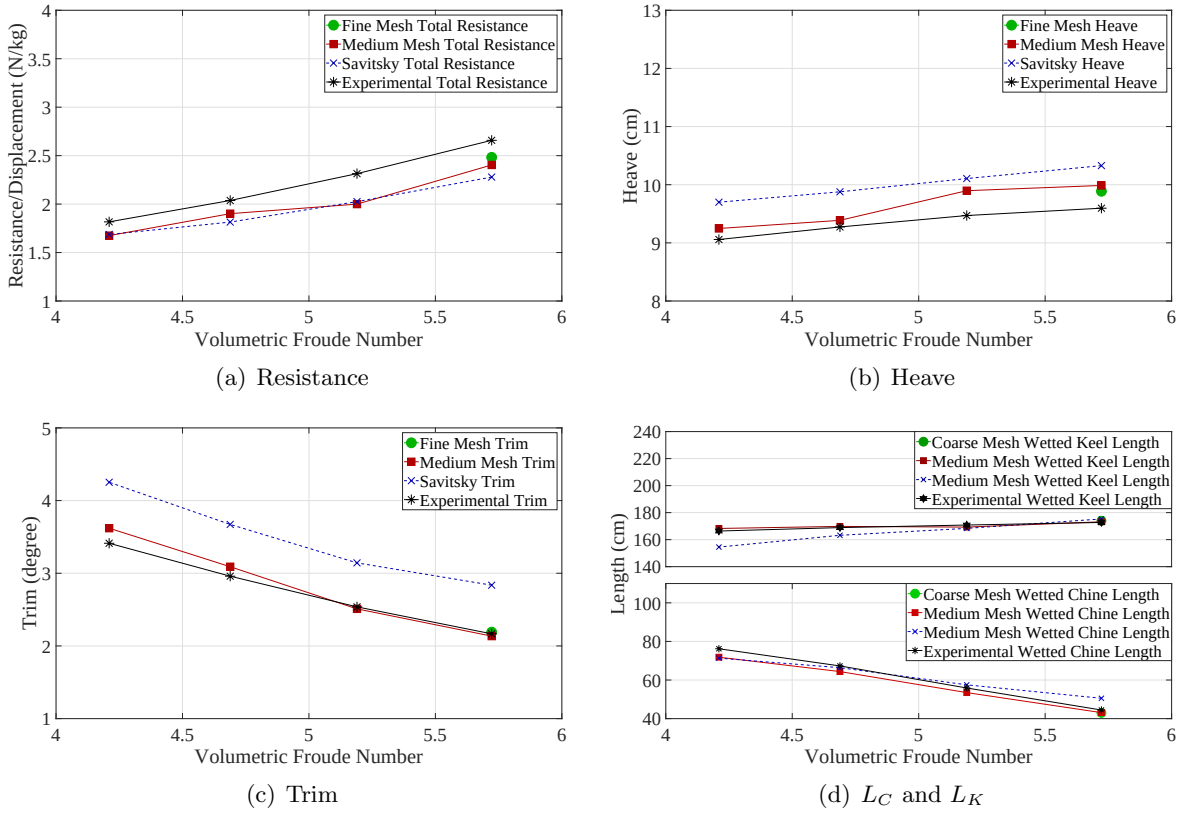

(a) Resistance (b) Heave

(c) Trim (d) L_C and L_K

Figure 8: Comparison Plot vs Volumetric Froude Number

this inaccuracy seems to be as marked as in the coarse grid case. VOF contours in the hull bottom pressure area suggest higher friction drag predicted by the medium mesh. However, this is not confirmed by results presented in figure 4(a). The reason might be related to the solution obtained in the spray area, in which the coarse grid predicts extensive ventilation (more extensive green/blue colors), while the medium and the fine resolution leads to higher values of γ (VOF). Pressure solution on the hull bottom is not significantly affected by grid resolution as demonstrated in figure 4(b) in terms of pressure drag and in figures 5(b),5(b) and 7(b) terms of pressure coefficient $C_P = \frac{p - \rho g h}{0.5 \rho v^2}$.

5 PREDICTIONS AT DIFFERENT SPEEDS

The mesh verification study and the assessment of the numerical uncertainty highlighted the necessity of using high mesh resolution close to the hull in order to capture the correct dynamic of the free surface and in general of the γ (VOF) on the spray and the pressure area of planing hulls. However the computational budget at our disposal is insufficient to perform a validation of CFD predictions in a wide range of volumetric Froude numbers (Fn_∇). For this reason we present results obtained using the medium mesh (see table 2) for the solution of the hydrodynamic problem at Fn_∇=4.210 ,Fn_∇=4.689, Fn_∇=5.190 and Fn_∇=5.723. Results are presented in figure 8 in terms of non-dimensional calm water resistance, $\frac{R_T}{\Delta}$ (figure 8(a)),

heave of the Center of Gravity (figure 8(b)), trim angle (figure 8(c)) as well as wetted lengths of the chine L_C and the keel L_K (figure 8(d)). CFD predictions of total resistance averagely underestimates experimental measurements of about 9.5%. This discrepancy is minimum at $Fn\nabla$=6.689 where CFD predictions are characterized by a relative error w.r.t. experiments of about 6.9%. A maximum discrepancy of 13.7% is experienced at Fn_∇=5.190. The average relative error of CFD predictions w.r.t. experiments is consistent with the numerical uncertainty estimation determined at the highest speed (Fn_∇=5.723) in section 4. The dynamic attitude of the planing hull is well predicted in the range of speeds considered in the present study. This is demonstrated in figures 8(b), 8(c) comparing the experimental with the numerically predicted dynamic heave motion and trim angle and in figure 8(d) where the wetted chine and keel length are compared at different volumetric Froude numbers.

6 CONCLUSIONS

The Generic Prismatic Bull tested at the NSWCCD provides a valuable opportunity to test numerical models and tune their parameters against a modern set of experiments. The grid verification study and numerical uncertainty assessment presented in this paper highlighted the complexities in accurately capturing the free surface dynamics in case of violent flows caused by high velocity and pressure fields. The problem of numerical ventilation was partially mitigated by increasing the grid resolution while keeping relatively high values of $y+$. However further studies are needed to understand the influence of wall functions on VOF diffusion on the pressure area of planing hulls and to characterize the importance of numerical solution of the partial differential equation describing the transport of VOF. The accuracy of the results obtained at different speeds is consistent with the relative error of CFD predictions w.r.t. experiments found using other CFD solvers.

Acknowledgements

The support of the Office of Naval Research, grant N00014-17-1-2344, is gratefully acknowledged. Computations were run on the high performance computing clusters of Virginia Tech Advanced Research Computing Center.

References

[1] Lars Larsson, Frederick Stern, and Michel Visonneau. *Numerical ship hydrodynamics: an assessment of the Gothenburg 2010 workshop*. Springer, 2013.

[2] Brizzolara S. and Villa D. Cfd simulations of planing hulls. In *Proceedings of the Seventh International Conference on High-Performance Marine Vehicles, HIPER 2010*, pages 16–24, Melbourne, 2010. Florida Institute of Technology.

[3] Gaggero S. Ferrando M. and Villa D. Open source computations of planing hull resistance. *Transactions of the Royal Institution of Naval Architects Part B: International Journal of Small Craft Technology*, 157:83–98, 2015.

[4] R. Broglia and D. Durante. Accurate prediction of complex free surface flow around a high

speed craft using a single-phase level set method. *Computational Mechanics*, 62:421–437, September 2018.

[5] Brizzolara S. and Federici A. Cfd modeling of planning hulls with partially ventilated bottom. In *The William Froude Conference: Advances in Theoretical and Applied Hydrodynamics Past and Future*, pages 1–17, London, 2010. Royal Institution of Naval Architects.

[6] Brizzolara S. and Serra F. Accuracy of cfd codes in the prediction of planning surfaces hydrodynamic characteristics. In *Proceedings of the 2nd International Conference on Marine Research and Transportation, ICMRT'07*, pages A:1–12, Italy, 2007. U. of Napoli Federico II.

[7] Luca Bonfiglio and Stefano Brizzolara. Amplitude induced nonlinearity in piston mode resonant flow: A fully viscous numerical analysis. *Journal of Offshore Mechanics and Arctic Engineering*, 140(1):011101, 2018.

[8] D.C. Wilcox. Reassessment of the Scale-Determining Equation for Advanced Turbulence Models. *The American Institute of Aeronautics and Astronautics (AIAA)*, 26:1299–1310, 1988.

[9] F.R. Menter. Zonal two equation k-ω Turbulence Models for Aerodynamic Flows. In *24th AIAA Fluid Dynamics Conference, July 6-9, Orlando, Florida*, page 2906, 1993.

[10] F.R. Menter. Two-equation eddy-viscosity turbulence models for engineering applications. *AIAA journal*, 32(8):1598–1605, 1994.

[11] C.W. Hirt and B.D. Nichols. Volume of fluid (VOF) method for the dynamics of free boundaries. *Journal of Computational Physics*, 39(1):201–225, 1981.

[12] R. Featherstone. *Rigid body dynamics algorithms*. Springer, 2014.

[13] Luca Bonfiglio and Stefano Brizzolara. Unsteady viscous flow with non linear free surface around oscillating SWATH ship sections. *WSEAS Trans. Fluid Mech*, 9:49–57, 2014.

[14] Weil C.R. Lee E. and Fullerton A. Experimental results for the calm water resistance of the generic prismatic planing hull (gpph). Technical report.

[15] OpenFOAM Foundation. *OpenFOAM user guide*. OpenFOAM Foundation, 2014.

[16] Luis Eça and Martin Hoekstra. A procedure for the estimation of the numerical uncertainty of cfd calculations based on grid refinement studies. *Journal of Computational Physics*, 262:104–130, 2014.